ORIGINAL ARTICLE

Vibration analysis of BLDC motor drive employing model reference adaptive controller

N. Veeramuthulingam[1,2] [ID] · **A. Ezhilarasi[1]** · **M. Ramaswamy[1]**

Abstract The drive industry ensembles the stable operation of the motor with a perspective to adapt to the needs of the application and ensure the required delivery of power. It necessitates measures for arbitrating both the electrical and mechanical disturbances through the use of feedback control mechanisms and bring out its ability to cater the desired performance. The paper introduces the theory of the model reference adaptive control (MRAC) with a view to minimize the effects of vibration of the brushless dc (BLDC) motor. The emphasis owes to reflect the regulatory disturbances in terms of regulating the speed and therefrom observe the variations in the cogging torque, which contributes to be the primary reason for inducing vibrations in the motor. The forces calculated from the torque output of the MRAC controller form the input to estimate the amplitude of displacement experienced by the BLDC motor. The study relies on the finite element method (FEM) based structural harmonic analysis for the motor, to realize the variations in the displacement corresponding to the output of the MRAC. The efforts relate to minimizing the cogging torque and therefrom bring out the efficacy of the MRAC over the conventional PI controller in being able to lower its effects over a range of vibrating frequencies and thus claim its suitability for use in similar other motor drives.

✉ N. Veeramuthulingam
  sethukumark@gmail.com

  A. Ezhilarasi
  jee.ezhiljodhi@gmail.com

  M. Ramaswamy
  aupowerstaff@gmail.com

[1] Department of Electrical Engineering, FEAT, Annamalai University, Annamalai Nagar, Chidambaram, Tamil Nadu, India

[2] Annamalai University, Chidambaram, Tamil Nadu, India

1 Introduction

The brushless dc (BLDC) motors offer to replace the conventional motors in view of being able to produce a larger torque and operate at higher speeds, besides offering longer operational life and good dynamic performance. The motors envisage being fit for variable motor speed applications due to their comparatively compact size and weight and hence find a place in aerospace, automotive, computer, medical, and electronics industries.

The BLDC motors characterized by surprisingly higher ripple in the torque and sustained acoustic noise appear to be afflicted by the cogging torque, produced by means of the circumferential issue of the attractive forces between the rotor magnet and the teeth of stator. It experiences vibrations within the shaft and becomes detrimental in being able to support a large variety of high-performance motion control applications (Dutta et al. 2016). The stator slots width in the outer rotor type BLDC motors significantly becomes liable to produce the cogging torque (Nizam and Waloyo 2013). The cogging torque creates ripples in the speed and torque together with acoustic and vibration noise in the sense it becomes significant to explore measures for reducing its effects. Among the two types that include the slotted and slot less motors, the latter with the Halbach array produces lower cogging torque without much reduction in the developed torque.

Though the influence of skew angle on reducing the cogging torque in Kim et al. (2009); Abbaszadeh et al. 2012) invites attention where in a first and third layers of the three-layer stator model the angular changes of slot opening

position, rather than the middle layer, which reflects to be worthy of consideration. The main cause of vibration has been seen to arise on account of the saliency of the stator and the rotor magnets, the ripple in the magnetic radial forces, the torque ripple and the current harmonics. Besides the aerodynamics, manufacturing defects and the rotor unbalancing have also been found to contribute to introduce vibrations in the motor (Mekkemthong et al. 1645).bThe torque ripple produced by the electrical drives has been realized as a source of vibration and reduced through a procedure by which a feed to the sinusoidal current is enabled for the spindle motor in the sinusoidal driving mode (Zhipeng et al. 2023).

The finite element analysis (FEA) has been used to study the effect of the rotor geometry on its natural frequencies and provide the effective values of the parameters. Bearings have been proven to generate cylindrical and conical vibration patterns at low frequencies, which frequently occur within the motor's working speed range. The study has been laid to illustrate that the shaft allowances an important effect on the natural frequencies and requires the shaft to be shorter with a large diameter with a purpose to Extend the operating speed range of the rotor bending modes (Mendizabal et al. 2021).

The tangential and radial magnetic forces' properties have been investigated and the external magnetic vibrations of an internal permanent magnet (IPM) motor produced by flux weakening control changes in the phase angle of applied current were examined (8). The Maxwell stress tensor approach was used to evaluate the magnetic force, and the mode superposition method was used to examine the vibrations caused by the application of a rotating magnetic force.

A simple test technique has been suggested for cogging ripple torque measurement by using the dynamometer, wherein a process of elimination was used to estimate the magnitude and Cogging torque periodicity at low speeds (9). A fault diagnosis scheme has been proposed for the choose trustworthy failure indications, the BLDC motor is based on vibration studies in several representative domains. A set of vibratory signals relating to a set of selective cases has been generated using analytical models and a procedure evolved for comparing to identify the existence of a defect, each selected indication has a decision threshold (Alameh et al. 2018).

A scheme through which the torque ripple in the PMBLDC motor has been shown to be minimized by increasing the input voltage to be greater than the back emf. Different methodologies have been suggested to boost the input voltage during the commutation period and reduce the torque ripple in the higher speed range of operation of the motor (Ponce-Silva et al. 2022).

The vibration analysis and motor current signature analysis (MCSA) have emerged as prominent methods for detecting various rotor and stator defects in PMBLDC motors. To simulate the occurrence of stator winding insulation breakdown, a short circuit has been established artificially between two windings. The diagnostics system has been proved to detect the stator failure and differentiate between different fault states using experimental data (Tanvir Alam Shifat 2020).

The review does not include a comprehensive examination of the modal analysis of motor components, implying the necessity for a structural analysis of the motor using the finite element approach.

2 Problem formulation

The focus owes to evolve a mechanism wherefrom it can strive to arrive at the output for the MRAC in order that it may serve to lower the cogging torque ripple and thus reduce the effects of the vibration on the motor. It attempts to lay the methodology on the FEM platform for relating the forces with the MRAC output and allow the closed loop error correction strategy to reduce the ripple in the torque and the cogging torque. The scheme evaluates the performance using both 2D and 3D analysis for illustrating the decrease in the amplitude of the vibration at different frequencies.

3 Proposed methodology

The reduction in the amplitude of the vibration displacements may be generated by without compromising the motor's performance, the appropriate parameter selection. It orients to increase the stiffness of the stator in a PMBLDC motor through a new structural design by shifting its natural frequencies to higher values and thereby enable a reduction in the effects of vibration.

The concept comprises combining JMAG software components with technology tools based on Finite Element Analysis for electric machine models, allowing co-simulation with circuit and control components simulation using external software (Veeramuthulingam et al., 2018). For varied geometries, it uses an eigenvalue technique to find Each natural frequency has a vibration mode assigned. It gets at the stator construction with defined slot parameters and gives the best values for operating with the highest natural frequencies in various mode shapes as well as

stiffness increase (Sheela et al., 2021). The natural frequencies may be altered by altering the characteristics, which has an impact on the system's size, inertia, and forces. The lower mode numbers in the different circumferential vibration modes and their associated natural frequencies become essential in analyzing the vibration's effect (Benedikt Kaiser 2022).

The proposed block diagram in the Fig. 1 outlines the circuit configuration, where in it shows the FEM of the BLDC motor drawing power from a solar PV source through a modified boost converter and a three phase VSI interfaces. It operates through exclusive closed loop control schemes with a perturb and observe (P and O) based maximum power point tracker (MPPT) in the front end to maximize available

resources and a model reference adaptive controller (MRAC) in the back end to try to reduce cogging torque.

The technique for analyzing various electromagnetic sources that cause stator vibration and evaluating the influence of motor stator structure include running vibration tests on the motor at the desired rotating speed under no load. It includes two acceleration sensors with one housed on the top of the motor and the other on the motor foundation being used for reference.

The load torque along with the corresponding electromagnetic torque form the two inputs, the output torque from the FEM serves to measure the cogging torque, which allows estimating the magnitude of the vibrations experienced by the motor under that operating state. In an attempt to minimize the cogging torque, the controller brings in the

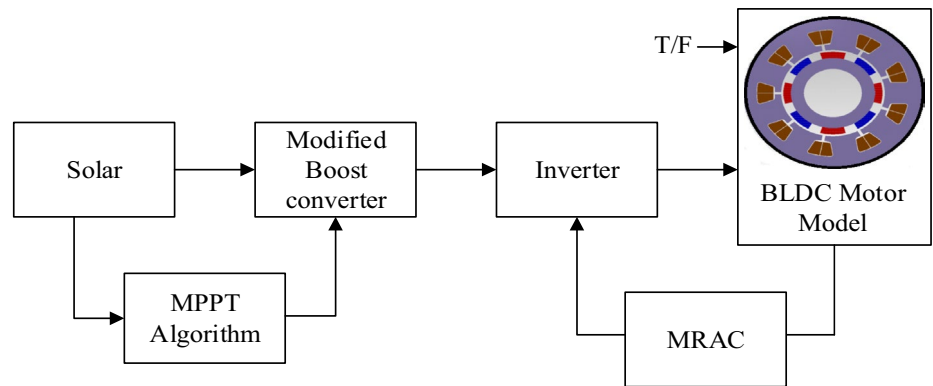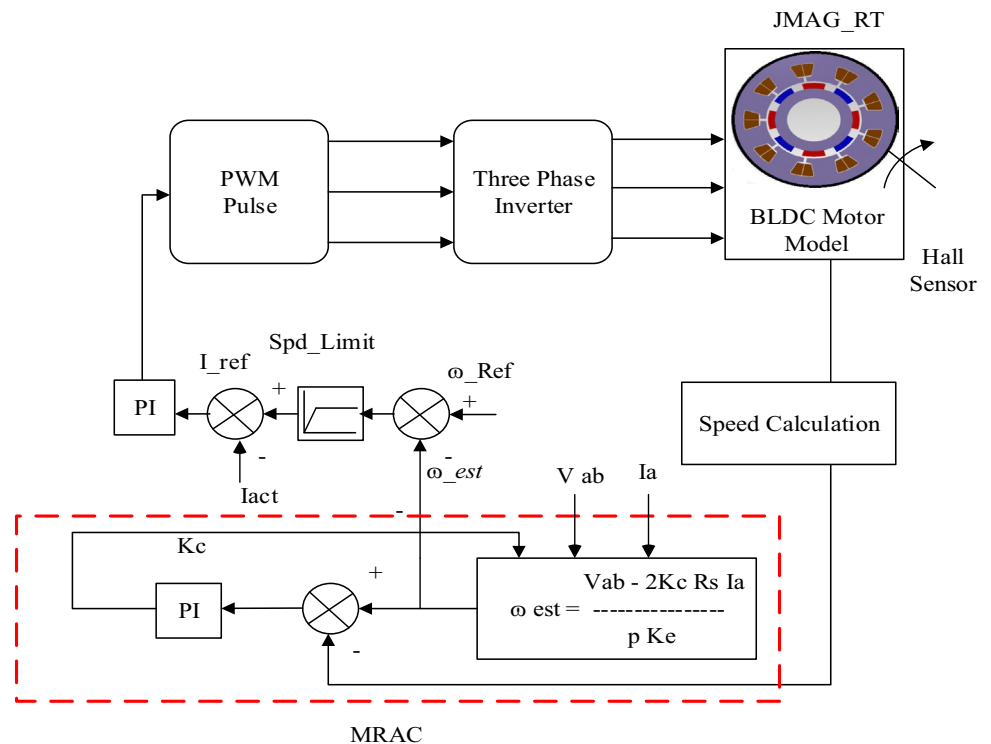**Fig. 1** Block Diagram of Proposed System

Fig. 2 Block Diagram of Complete Proposed System

necessary correction by reshaping the current with a view to reduce the ripple in the torque and therefrom enable the lowering of the cogging torque.

The use of the MRAC gathers strength particularly in places where it requires to follow a theory of adaptive manipulations. The strategy explained using the Fig. 2 relates to the purpose of regulating the speed and exercising a control over the current. The stator current calculated using the d-q frame, on being converted to compute the speed error facilitates the generation of the PWM pulses for the power switches in the VSI together with a triangular carrier wave. It constitutes to be a twin loop system with a regulator in the speed loop and a current variable controller for minimizing the torque ripple.

It uses JMAG-Express to create a modified geometry of the BLDC motor test model based on the existing motor template, as shown in Fig. 3. It entails choosing core materials for the stator and rotor from the categories of steel, magnetic materials and isotropic. With the chosen motor specifications and on the simulation being run the FEA calculates the cogging torque as as indicated by Eqn. the total of interactions between each of the rotor PMs' edges, as well as the stator slots (1).

From the expression in Eqn. the cogging torque for the BLDC machine can be calculated analytically (2)

$$\text{Tc} = -\frac{gL_i}{\mu_0}\frac{D_{1in}}{2}A_T\frac{B_{mg}}{k_c}\sum_{k=1,2,3}(-1)^k\varsigma_k\sin\left(k\frac{\pi}{t_1}c_t\right)\sin\left(\frac{2k\pi}{t_1}X\right) \tag{1}$$

where B_{mg} refers to D1 is the inner diameter of the stator, g is the air gap, kc is the carter's coefficient, and 0 is the magnetic permeability of free space, all of which are related through expressions in the Eqns. (3) in order (11)

$$k_c = \frac{t_1}{t_1 - \gamma g'} \tag{2}$$

$$g' = g + h_m/\mu_{rec} \tag{3}$$

hm height of PM, g equivalent air gap:

$$\varsigma_k = k_{ok}k_{skk} \tag{4}$$

kskk is stator slot skew factor refer to slot pitch $t1$:

$$A_T = -2\gamma\frac{g'}{t_1}B_{mg} \tag{5}$$

$$\sigma = \frac{b_{14}}{g'} \tag{6}$$

$$\gamma = \frac{4}{\pi}\left[0.5\sigma\arctan(0.5\sigma) - \ln\sqrt{1+(0.5\sigma)^2}\right] \tag{7}$$

$$\rho = \left(\frac{\sigma}{5+\sigma}\right)\frac{2\sqrt{1+\sigma^2}}{\sqrt{1+\sigma^2}-1} \tag{8}$$

$$k_{ok} = \frac{\sin[k\pi\rho b_{14}/(2_{t1})]}{k\pi\rho b_{14}/(2t_1)} \tag{9}$$

$$k_{skk} = \frac{\sin[(kb_{sk}\pi/t_1)]}{(kb_{sk}\pi/t_1)} \tag{10}$$

$$c_t = t_1 - b_{14} \tag{11}$$

where $t1$ represents the slot pitch and X the rotor position.

When the racial tensions on the stator poles match the natural vibration, the motor vibrates (Fei and Luk 2011).
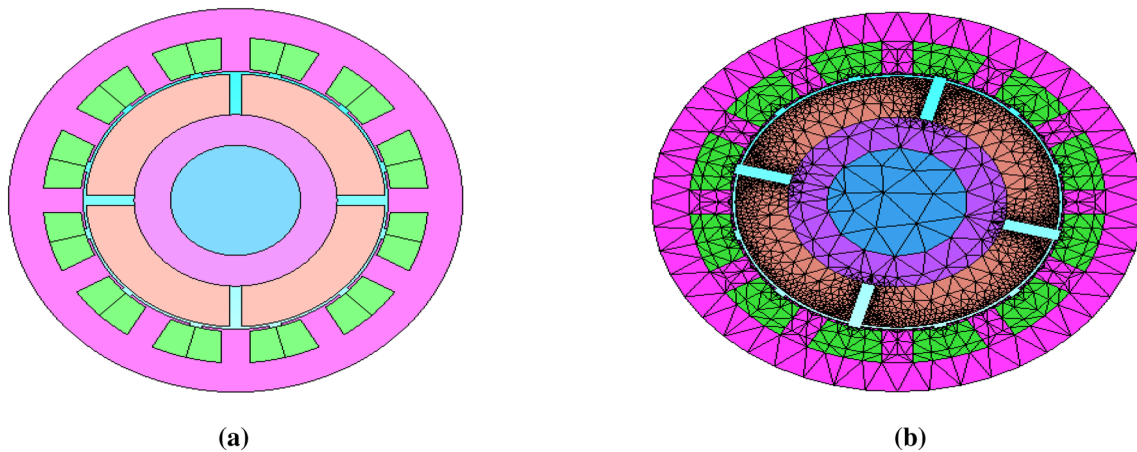

Fig. 3 JMAG -RT view of PMBLDC motor **a** model **b** mesh

Table 1 Basic parameters of PMBLDC motor

S. no	Parameter	Value
1	Power (Watts)	1320
2	Voltage (Volts)	310
3	Speed (Rpm)	3000
4	No of poles	4

Table 2 Stator parameters of PMBLDC motor

Stator	
Number of Slots	12
Inside Diameter	30.58 mm
Outside Diameter	59.95 mm
Length of stator core	59.95 mm
Slot Opening Width	1.848 mm
Tooth Width	4.059 mm
Tooth Tang Depth	0.9146 mm
Core Back Width	7.012 mm
Stacking factor	95

Table 3 Rotor parameters of PMBLDC motor

Rotor	
Number of Poles	4
Outside Diameter, mm	30
Outside Diameter of Rotor Core, mm	20.7
Gap between Magnets, mm	1.32
Number of Turns	80

Table 4 Materials details of PMBLDC motor

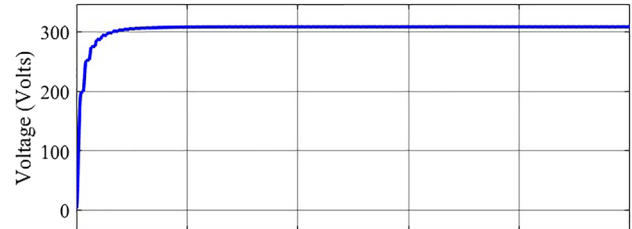| Components	Materials	Density, kg/m^3
Stator Core and Rotor Core	JSOL—Steel_Sheets (50A1000)	7850
Coil	Copper	8960
Rotor Magnet	JSOL—NdFeB_Magnet	7500

Fig. 4 Output Voltage of Modified Boost Converter

Table 5 Voltage Ripple of Modified Boost Converter

Duty cycle	Voltage ripple
0.7	0.856
1.4	0.786
2.1	0.681
2.8	0.619
3.5	0.526
4.2	0.519

The vibration modes are caused by opposite pairs of stator teeth bending and deforming due to the torque in the motor. The FEA formulation for the static analysis may be related by the Eqns. (12) and (13).

$$[K][U] = [F] \qquad (12)$$

$$[U] = [U]^{-1}[F] \qquad (13)$$

The stiffness matrix is [K], the force vector is [F], and the displacement vector is [U]. The resulting displacement vector of the body in the FEA is computed using the Eq. (12). The FEM was created in the ANSYS environment using BRICK 87 element characteristics for 3D elements and meshes for the specified dimensions. Figure 1 shows a mesh model (3) that chooses a displacement boundary that is determined by the shaft's two ends and set to zero.

4 Simulation

It orients to examine the performance of the solar PV powered PMBLDC motor system on a MATLAB/Simulink platform with JMAG environment. The Tables 1, 2, 3 and 4 include the specifications of the motor, dimensions of the stator and the rotor and the type of the material used for manufacturing motor. The Fig. 4 shows the regulated output voltage of the modified boost converter obtained from the Solar PV source at the irradiation, level of 1000 W/m^2 and the Table 5 includes the corresponding ripple in the dc link voltage, expressed as a function of the variation in the load torque. The closed loop MPPT controller assuages to extract the maximum power at each operating point and in addition contributes to reducing the voltage ripple.

The time variation of the solar output, modified boost converter voltage, inverter output voltage, stator current, torque and the speed of the motor seen in the Figs. 5 and 6 relate to the two chosen operating points of 0.7 Nm and

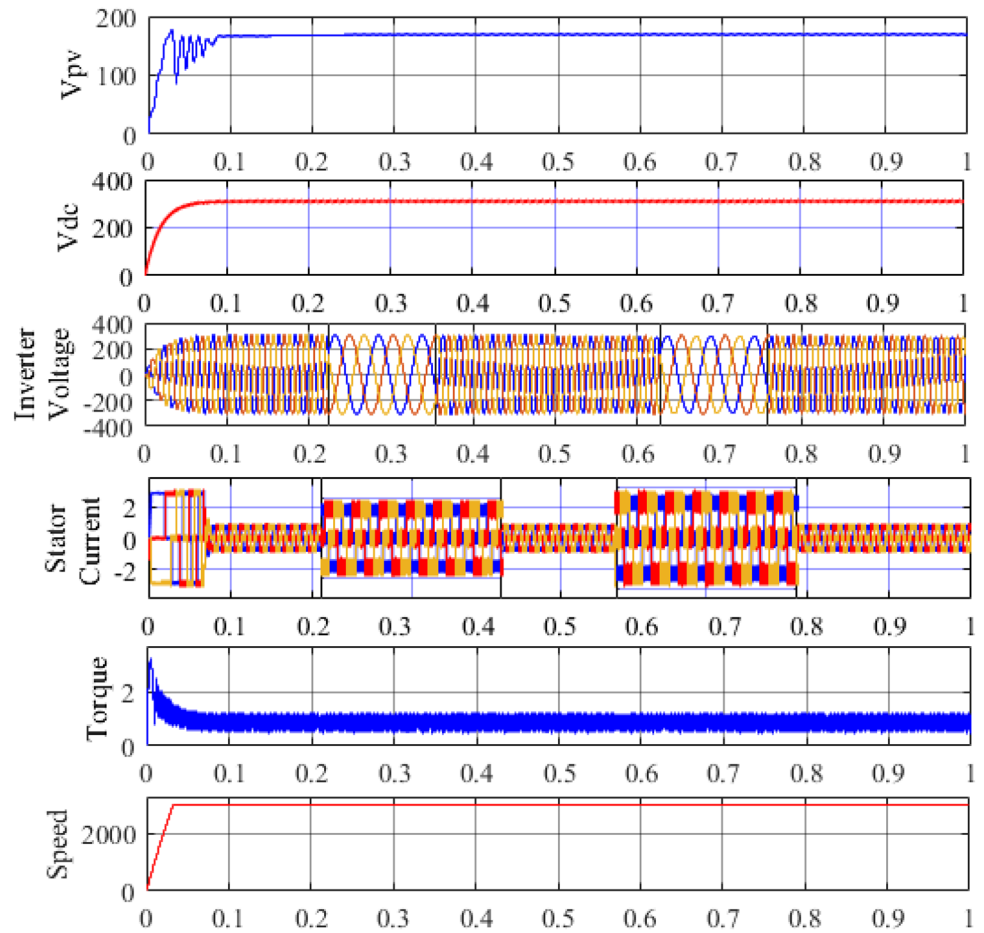**Fig. 5** Steady state and regulatory response at 0.7 Nm (Sheela et al. 2021)

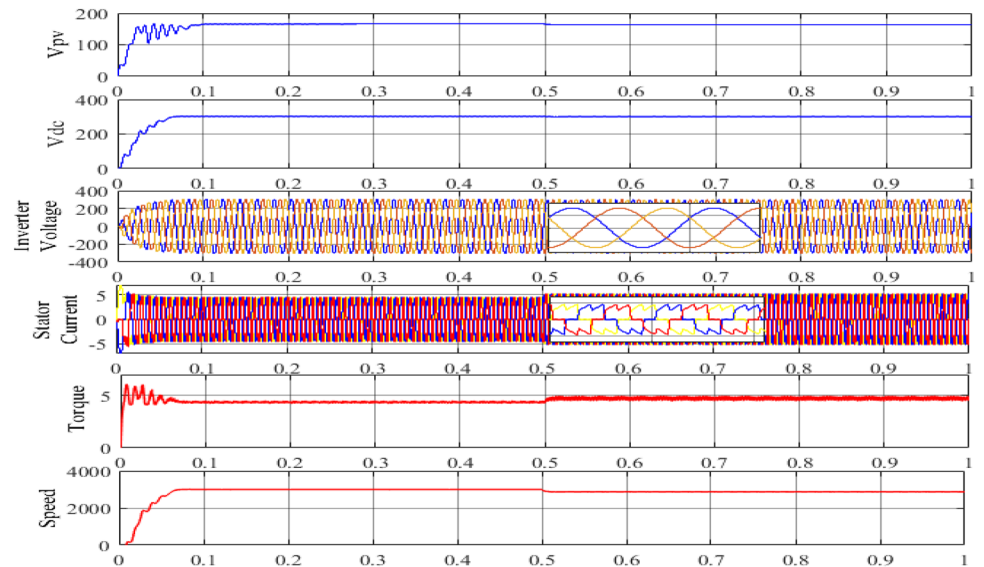**Fig. 6** Steady state and regulatory response at 4.2 Nm (Sheela et al. 2021)

Fig. 7 Cogging Torque at 0.7 Nm (Kurinjimalar et al. 2021; Veeramuthulingam et al. 2018)
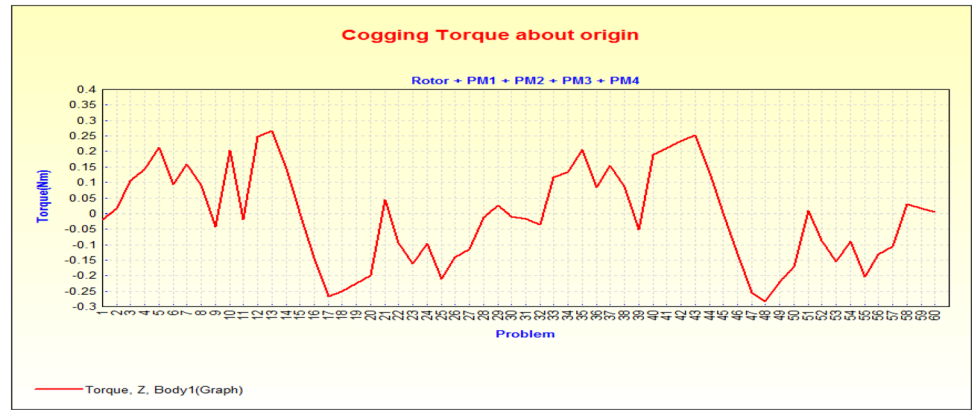

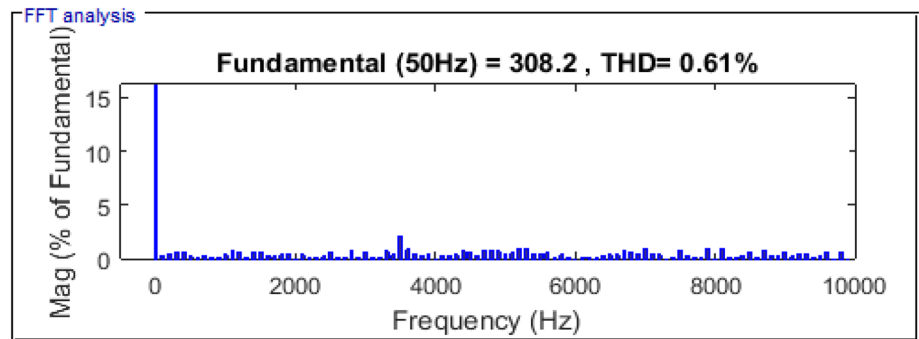**Fig. 8** THD Spectrum of Inverter Output Voltage (Sheela et al. 2021)

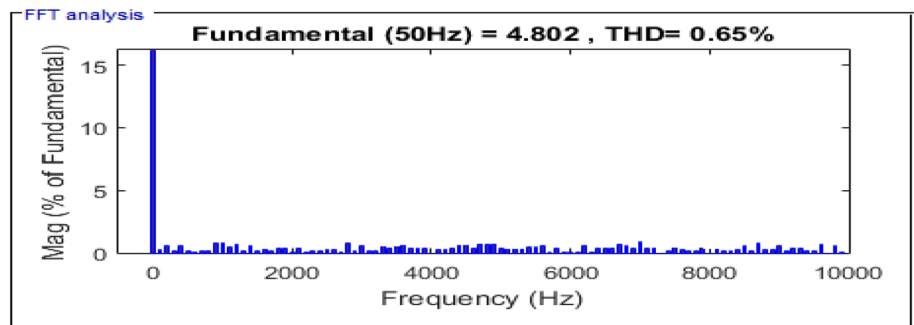**Fig. 9** THD Spectrum of Stator Current (Sheela et al. 2021)

Fig. 10 Cogging Torque of PMBLDC Motor at 4.2 Nm (Kurinjimalar et al. 2021; Veeramuthulingam et al. 2018)
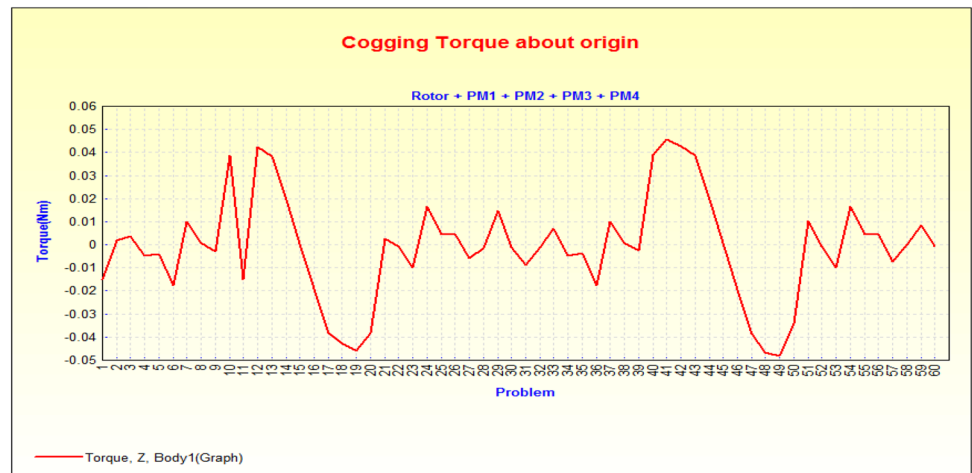
Table 6 Performance Comparison

Load (Nm)	Inverter voltage THD		Stator current THD		Speed (RPM)		Torque Ripple From MATLAB		Cogging Torque	
	PI	MRAC	PI	MRAC	PI	MRAC	PI	MRAC	PI	MRAC
0.7	5.30	5.10	5.74	5.20	3000	3000	6.679	5.711	6.78	4.64
1.4	4.73	4.51	4.56	4.24	2997	2999	6.146	5.310	4.86	3.96
2.1	3.76	3.65	3.80	3.26	2996	2998	5.595	4.493	3.91	2.95
2.8	2.10	2.06	2.76	2.58	2994	2997	4.810	3.908	3.06	1.60
3.5	1.32	1.25	2.13	1.10	2992	2997	3.92	3.217	2.14	0.68
4.2	0.78	0.61	1.02	0.65	2990	2995	3.418	3.015	1.23	0.195

4.2 Nm (Sheela et al. 2021). It further brings out that on the introduction of a sudden 10% increase at 0.5 secs in both the cases that while the speed remains regulated at its rated value, the voltage, current and the torque settle at their new steady state values owing to the action of the MRAC. The Fig. 7 reflects the variation of the cogging torque experienced by the motor corresponding to the operating point no f 0.7 Nm.

The THD spectra displayed in the Figs. 8 and 9 respectively correspond to the inverter output voltage and the stator current drawn at the operating point of 4.2 Nm establish the merits of the MRAC in being able to increase their fundamental components (Kurinjimalar et al. 2021). The smaller magnitude of the cogging torque calculated at the same operating point as noticed from its variation in the Fig. 10 obtained through the use of the JMAG software further augurs the benefits of the MRAC.

The simulation readings in the Table. 6 elaborate the performance of the MRAC over the conventional PI in the sense it extracts closer regulated values for the speed, smaller THD values for the inverter voltage, the stator current and the torque ripple and lower values for the cogging torque over the operating of the load torques.

5 Vibration analysis

FEA machine models exported to Simulink for more realistic evaluations of the control algorithms give the apparent benefit of low-cost simulations as compared to costly and risky physical system prototype testing. On the other hand, the time required for co-simulation as a result of completing the FEA model calculations using the time step for the control system simulation might be an issue. An alternative method is to use ANSYS Simplorer to co-simulate the complex model of the electric machine. With the adaptable JMAG-Designer environment, the JMAG user interface

excels at handling multiple scenarios from the same fundamental model. The JMAG Designer Version 12.0 software enables the electrical and magnetic field analysis during its steady state and transient operation.

The exercise continues to develop the FE model of the PMBLDC motor in the ANSYS environment with the given dimensions of the stator material made from M19 steel. It meshes the model using 2D and 3D elements and carries out the modal analysis to extract five mode frequencies. The displacement magnitudes of the model estimated there from as shown in the Figs. 11a–e and 12a–f respectively relate to the vibrating frequencies corresponding to the five modes included in the Table 7.

The deformation due to the electromagnetic forces experienced by the stator creates a gap and its corresponding change may affect the electromagnetic fields and thus the calculation of vibration amplitudes assumes significance. The design of a stator and the periods of repeated forces can impact its vibration, causing harmonic vibrations to synchronize with periodic-repeated electromagnetic forces. When the stator vibration amplitudes become relatively modest, the amplitude of the stator vibration can be assumed to be a linear superposition of its natural modes and the Fig. 13a and b show the amplitude of the vibration of the motor for the different modes in the X and Y directions respectively (Table 8).

6 Piezoelectric accelerometers

The oscillation force applied to the defective zone defines the fault, and the force is linearly related to the oscillation acceleration. Piezoelectric accelerometers are useful for measuring and controlling vibration. Both the vibration-acceleration and the vibration-velocity are frequently measured for diagnostic purposes in constrained low frequency ranges.
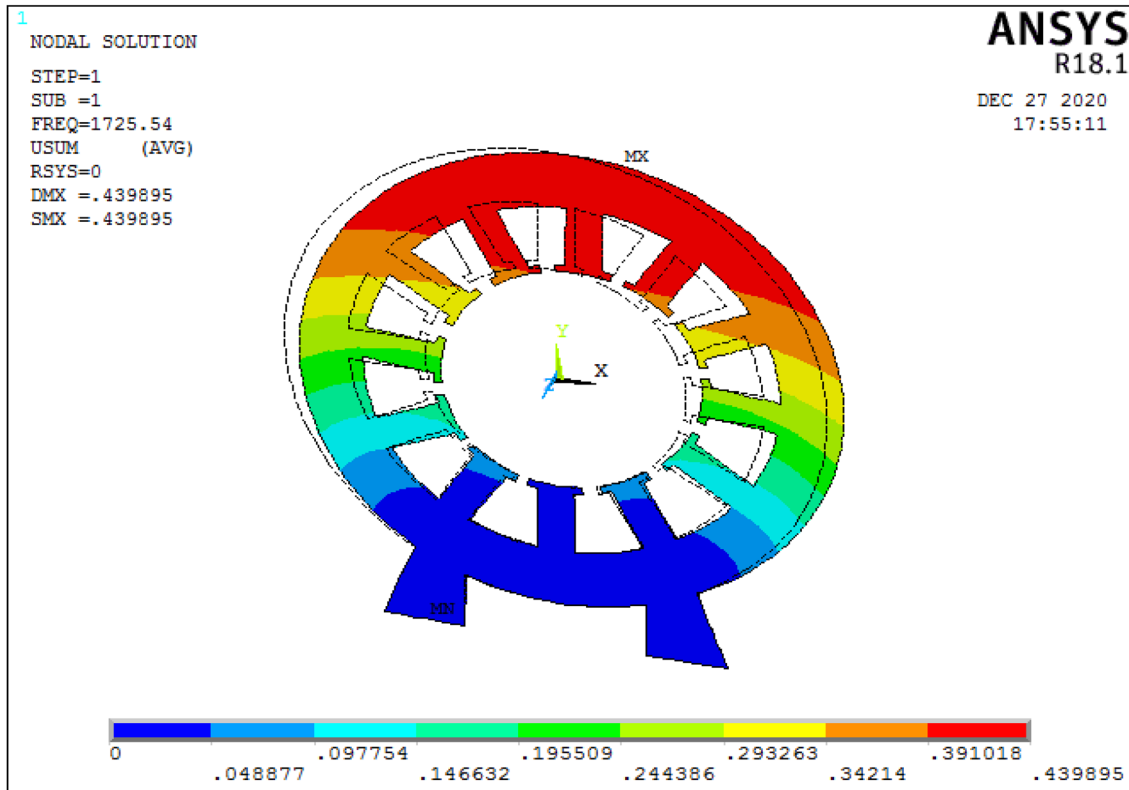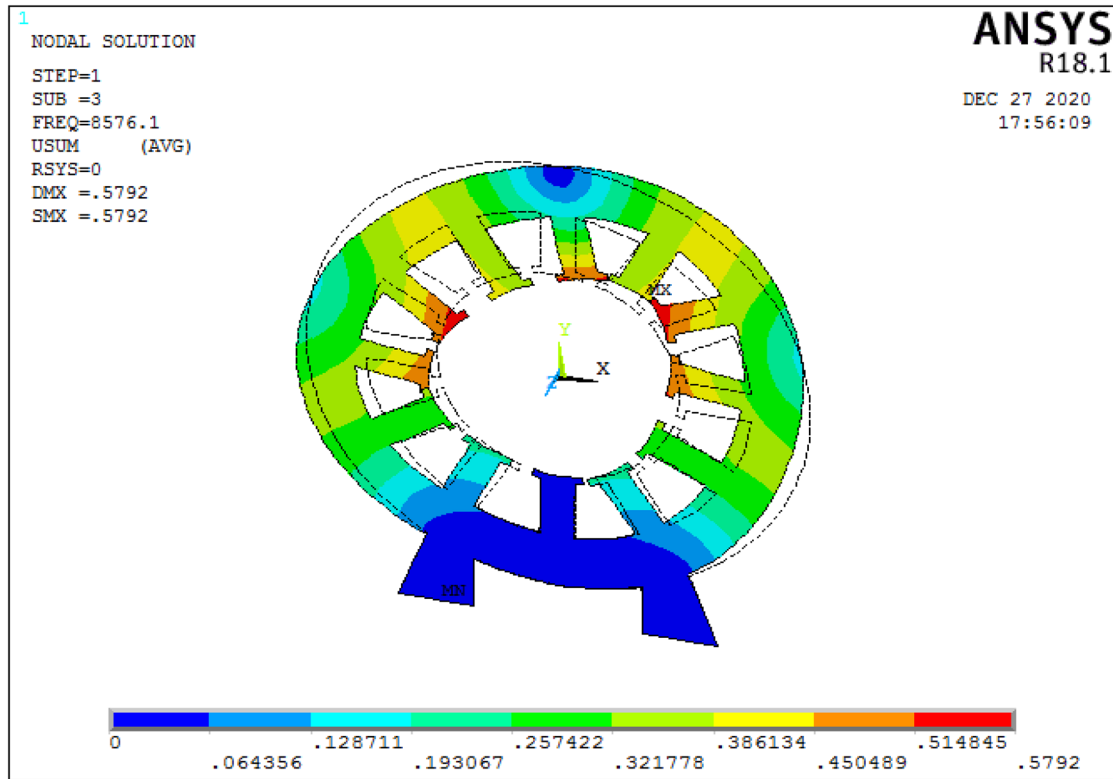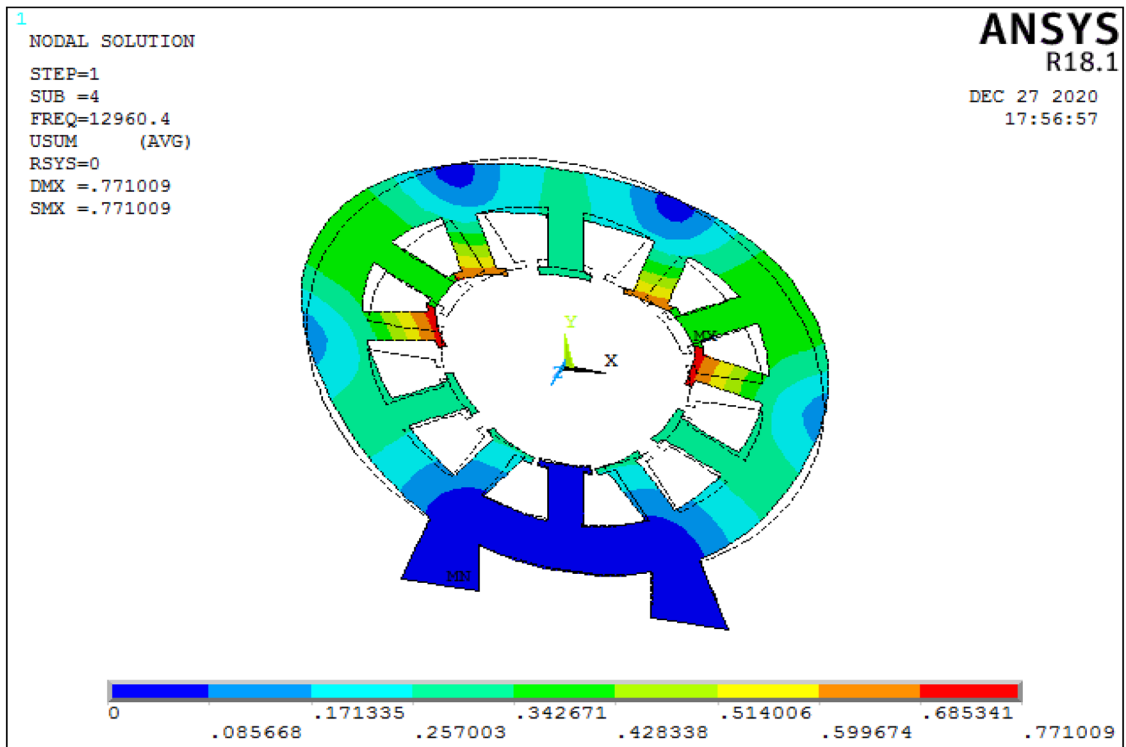
(a) Mode 1
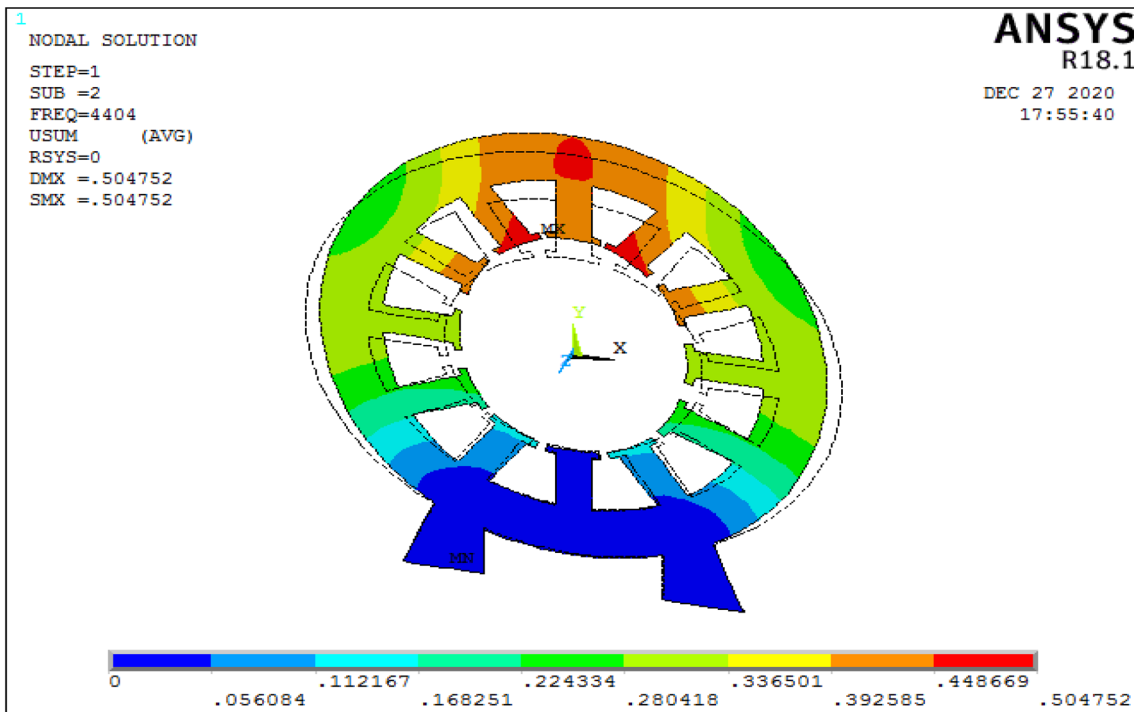
(b) Mode 2

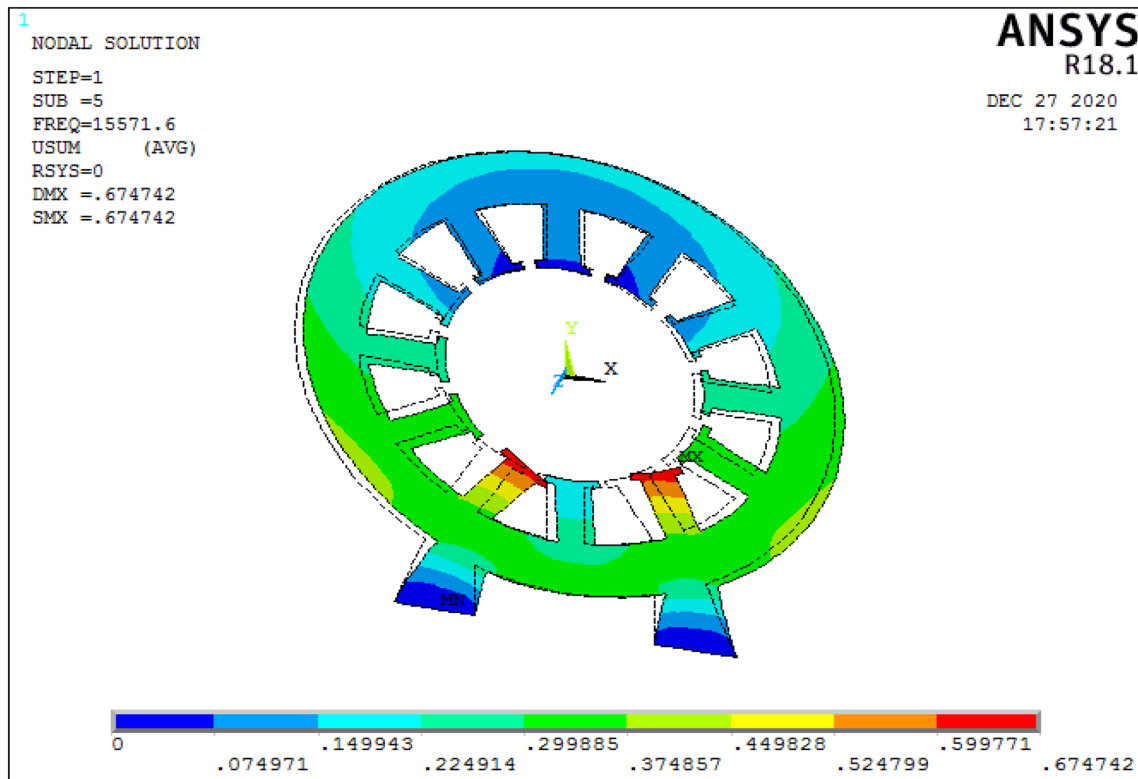**Fig. 11** a–e different mode frequencies and their shape in 2D (Puttalakshmi and Paramasivam 2013)

(c) Mode 3

(d) Mode 4

Fig. 11 (continued)

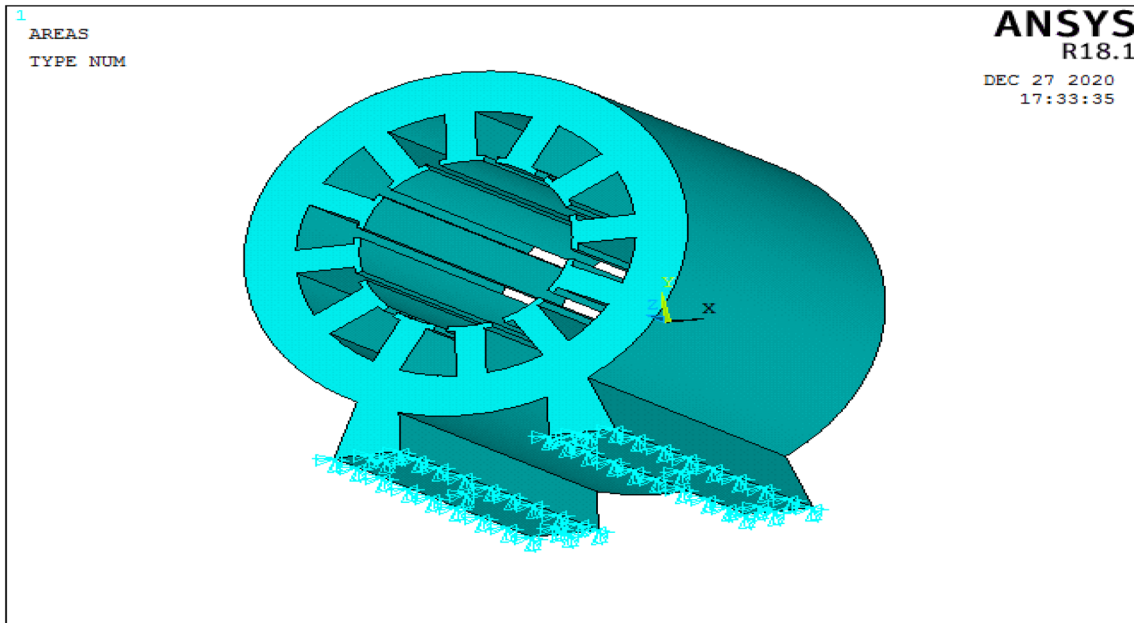**(e)** Mode 5

Fig. 11 (continued)

The majority of vibration measurements typically employ piezoelectric effect-based vibration-acceleration sensors. The output electric charge for these types of sensors is proportional to the force acting on the sensor. Electric signals are created from the vibration signal. This signal needs to be analyzed without losing the diagnostic data. The following tasks must be carried out by the vibration analysis equipment:

• Measuring the overall vibration level using the units specified by these standards, within a prescribed frequency range.

• FFT-based spectral analysis of the vibration.

• Examination of the oscillation power of various vibrational elements that were initially extracted from the vibration signal.

FFT is used to create harmonic vibration spectra from data gathered by the accelerometer. A time-domain signal's frequency domain representation can be extracted using the Fast Fourier Transform (FFT), a mathematical operation.

7 Conclusion

The theory of the MRAC has been introduced to reduce the effects of the vibration in the PMBLDC motor through an attempt of lowering the ripple in the torque and the cogging torque. The controller has been laid to offset the sudden change in the load torque using its feedback methodology and in turn minimize the amplitude of the displacements. The performance has been evaluated from the FEM based structural harmonic analysis in the ANSYS environment. The simulation results have been projected to claim the torque ripple reduction in the MATLAB platform and the cogging torque both using 2D and the 3D analysis in the ANSYS medium wherefrom it augurs a minimization effect to the vibration of the motor.
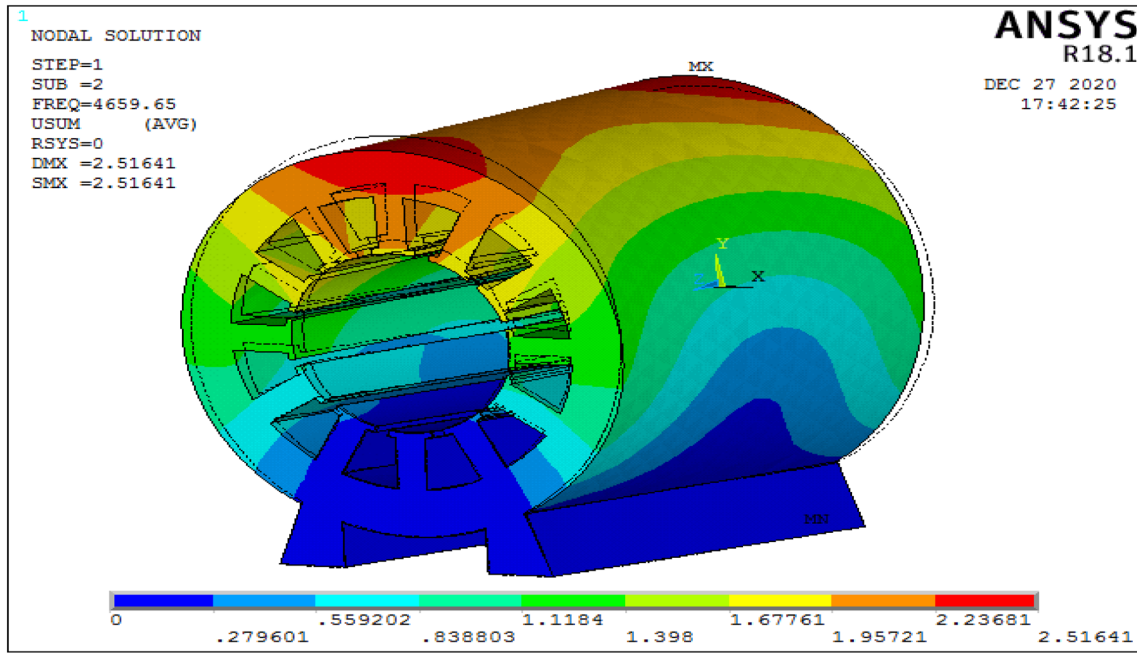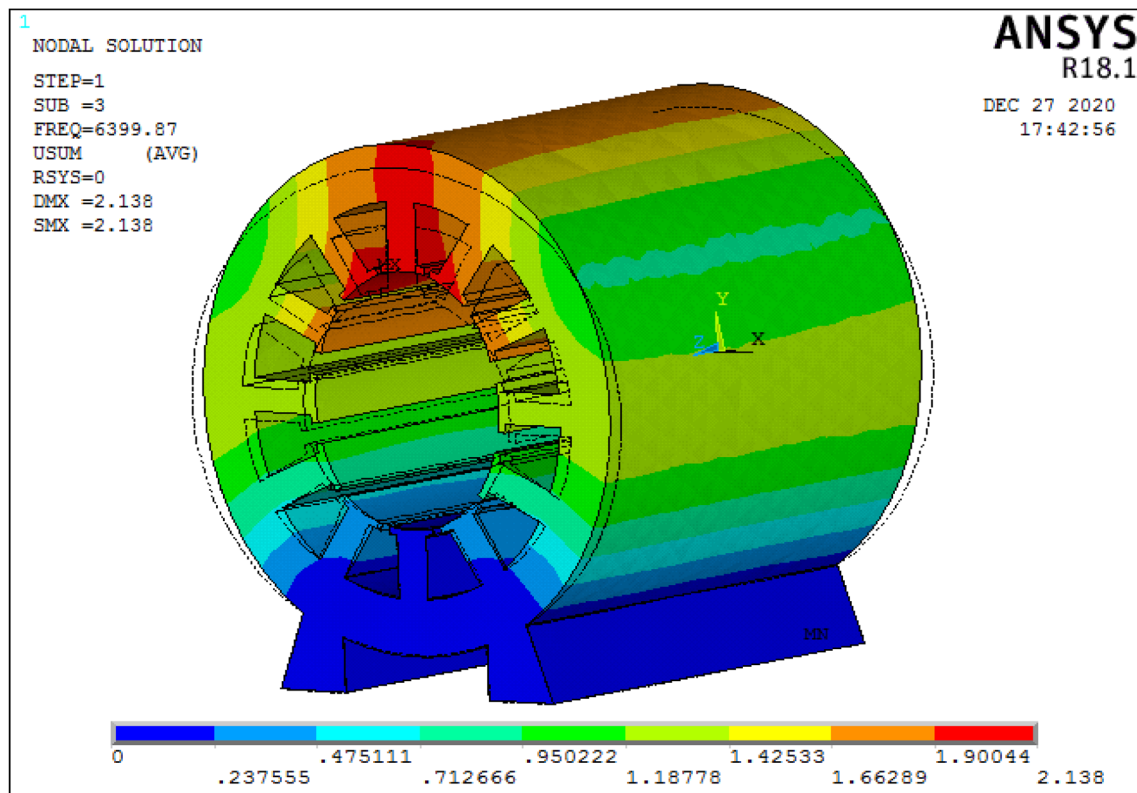
(a) Boundary condition
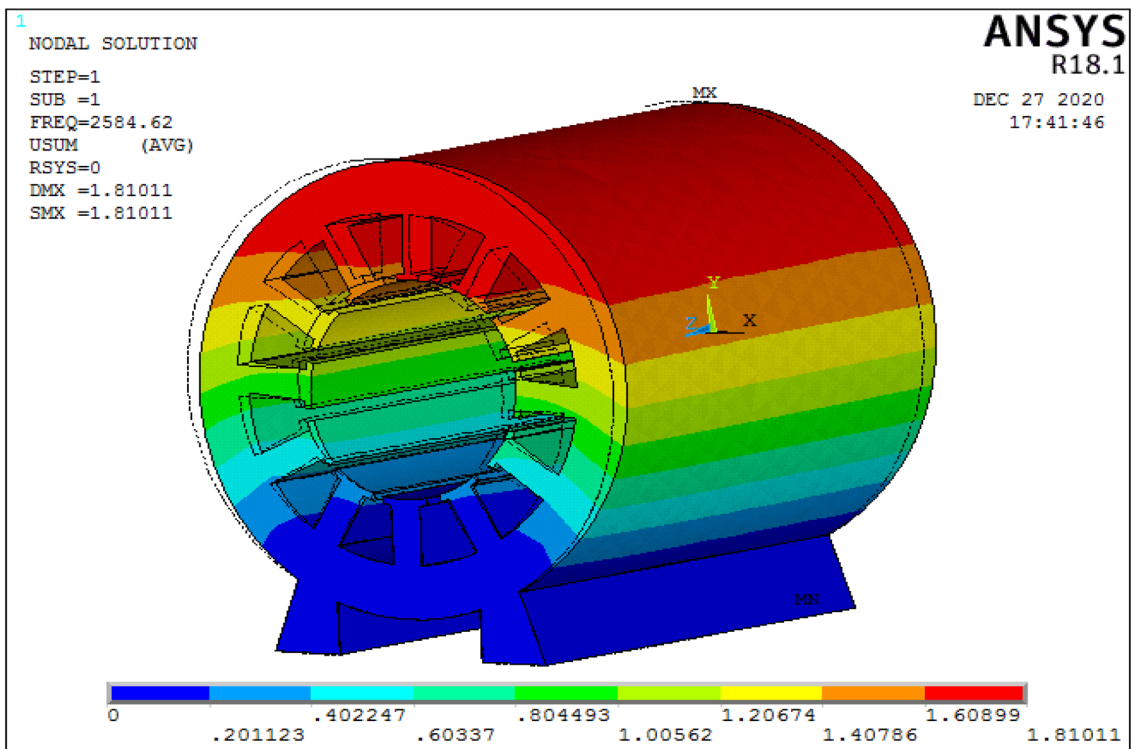
(b) Mode 1

Fig. 12 **b–f** different mode frequencies and their shape in 3D (Puttalakshmi and Paramasivam 2013)
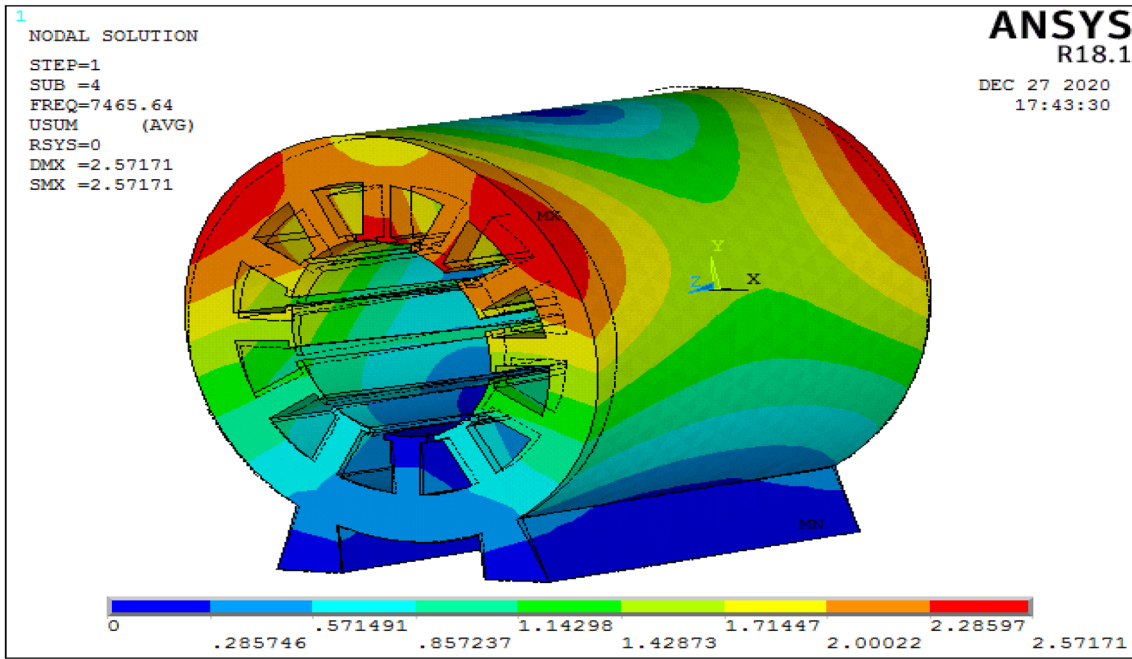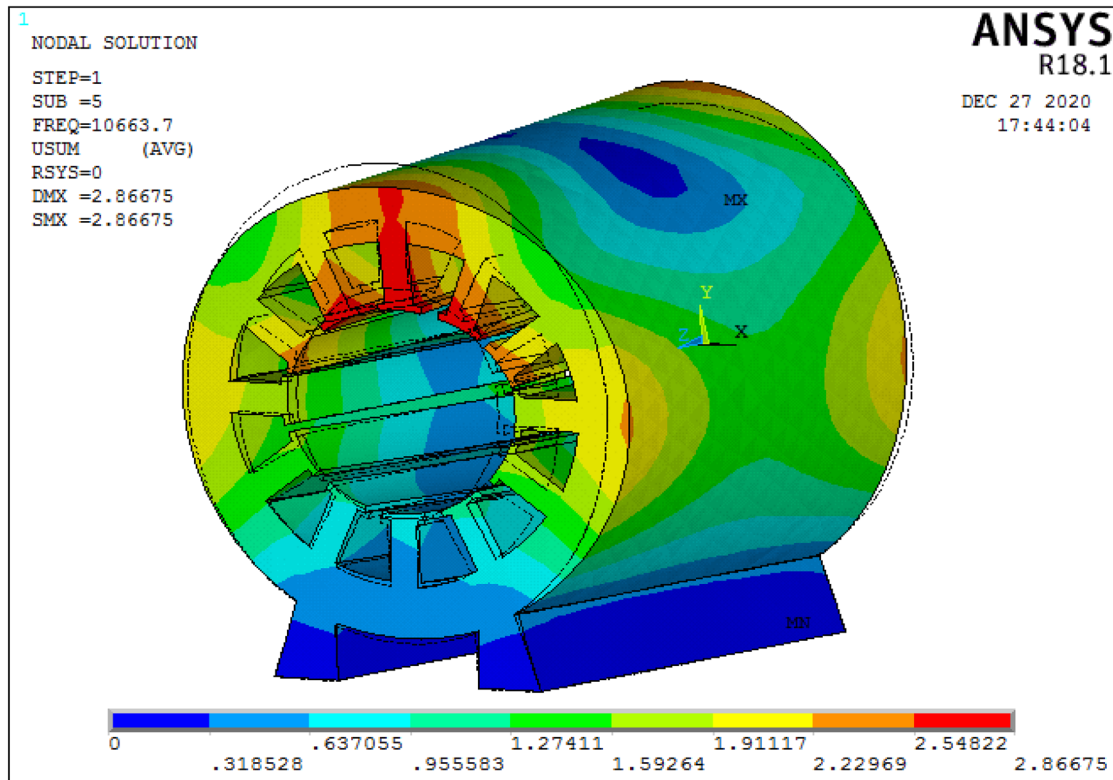
(c) Mode 2

(d) Mode 3

Fig. 12 (continued)

(e) Mode 4

(f) Mode 5

Fig. 12 (continued)

(a) MRAC_ X Direction [22]
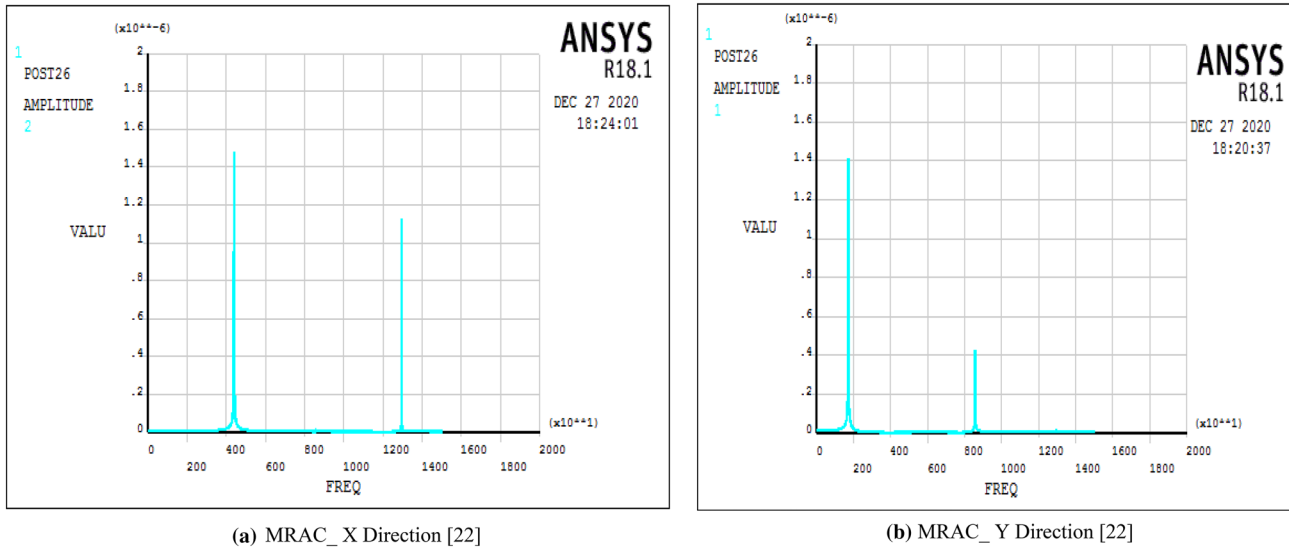

(b) MRAC_ Y Direction [22]

Fig. 13 **a** MRAC_ X Direction (Puttalakshmi and Paramasivam 2013) **b** MRAC_ Y Direction (Puttalakshmi and Paramasivam 2013)

Table 7 Vibration frequencies for both 2D and 3D for different mode

S. no	No of modes	2 D	3D
1	1	1725 Hz	2584 Hz
2	2	4044 Hz	4659 Hz
3	3	8576 Hz	6399 Hz
4	4	12,960 Hz	7465 Hz
5	5	15,571 Hz	10,663 Hz

Table 8 Vibration analysis

Frequency (Hz)	Displacement	
	Proposed paper	Reference paper 23
80	0.0008	0.0006
160	0.0026	0.0022
240	0.0059	0.0051
320	0.0100	0.0090
400	0.0165	0.0141
480	0.0268	0.0203
560	0.0298	0.0277
640	0.0421	0.0362

Declarations

Conflict of interest The authors declare that there are no known conflicts of interest associated with the work presented in this manuscript.

Human participants and/or animals This section does not apply.

Informed consent No Human cells and/or animals were used as part of this research. Hence this section is not applicable.

References

Abbaszadeh K, Alam FR, Teshnehlab M (2012) Slot opening optimization of surface mounted permanent magnet motor for cogging torque reduction. Energy Convers Manage 55:108–115

Alameh K, Hoblos G, Barakat G (2018) Statistical vibration-based fault diagnosis approach applied to brushless DC motors. IFAC 51(24):338–345

Dutta R, Ahsanullah K, Rahman F (2016) Cogging torque and torque ripple in a direct-drive interior permanent magnet generator. Progress in Electromagn Res B 70:73–85

Fei W, Luk PCK, Shen JX, Xia B, Wang Y (2011) Permanent magnet flux-switching integrated starter generator with different rotor configurations for cogging torque and torque ripple mitigations. IEEE Trans Indus Appl 47(3):1247–1256

Ghemari Z (2018) Progression of the vibratory analysis technique by improving the piezoelectric sensor measurement accuracy. Microw Opt Technol Lett 60:13–14

Ghemari Z, Belkhiri S (2021) Mechanical resonator sensor characteristics development for precise vibratory analysis. Sensing and Imaging 22(1):40

Ghemari Z, Saad S, Khettab K (2019) Improvement of the vibratory diagnostic method by evolution of the piezoelectric sensor performances. Int J Precis Eng Manuf 20:1361–1369

Ghemari Z, Salah S, Defdaf M (2021) Appropriate Choice of Damping Rate and Frequency Margin for Improvement of the Piezoelectric Sensor Measurement Accuracy. J Adv Manuf Syst 20(03):537–548

Guettaf A, Benchabane F, Bahri M (2014) Torque ripple minimization in switched reluctance motor using the fuzzy logic control technique. Int J Syst Assur Eng Manag 5:679–685

Jafarboland M (2018) Hossein Bagherian Farahabadi, "Optimum design of the stator parameters for noise and vibration reduction in BLDC motor." IET Electr Power Appl 12(9):1297–1305

Kaiser B, Parspour N (2022) Transverse flux machine—a review. IEEE Access 10:18395–18419

Kim DH, Choi JH, Son CW (2009) Theoretical analysis and experiments of axial flux PM motors with minimized cogging torque. J Mech Sci Technol 23:335–343

Kurinjimalar L, Balaji M, Prabhu S, Umadevi R (2021) Analysis of electromagnetic and vibration characteristics of a spoke type PMBLDC motor. J Electr Eng Technol 16(5):2647–2660

KangSoo Lee, JongKwang Kim, YongKeun Lee, (2018) "A Simple Method of Measuring Cogging Torque in BLDC Motors Using Dynamometer", In: IEEE International Conference on Consumer Electronics - Asia (ICCE-Asia) 24–26

Mekkemthong P, Chiangchin K, Suwankawin S (2011) Reduction of torque ripple and mechanical vibration of spindle motors in hard-disk drives using a sinusoidal driver. Microsyst Technol 17:1645–1652

Mendizabal M, McCloskey A, Poza J, Zarate S, Iriondo J, Irazu L (2021) "Optimum slot and pole design for vibration reduction in permanent magnet synchronous motors modeling design and control of electric machines. Appl Sci 11:4849. https://doi.org/10.3390/app11114849

Nizam M, Waloyo HT, and Inayati, "Design of optimal outer rotor brushless dc motor for minimum cogging torque Joint International Conference on Rural Information & Communication Technology and Electric-Vehicle Technology (rICT & ICeV-T), Bandung-Bali, İndonesia, pp1–4, 2013.

Ponce-Silva M, Olivares-Peregrino VH, De Leon-Aldaco SE (2022) A review of torque ripple reduction design methods for radial flux PM motors. Eng 3:646–661

Prabhu S, Chandrasekar V, Karthikeyan P, Lenin C (2012) Vibration and thermal analysis of switched reluctance hub motor. Eur J Sci Res 68(1):12–20

Puttalakshmi GR, Paramasivam S (2013) Electromagnetic flux analysis of permanent magnet brushless DC motor using magnet software. Int J Eng and Technol (IJET) 5(4):3215–3222

Saranya S, Balaji M (2019) Electromagnetic and vibration analysis of E-core switched reluctance motor with permanent magnets and auxiliary windings. J Power Electr 19(2):540–548

Sheela A, Atshaya M, Revathi S, Jeyapaul Singh N (2021) "Investigation on PMSM for electric vehicle applications using co-simulation of MATLAB and magnet software", IOP Conf. Series: Materials Science and Engineering Vol.1055, Issue. 012138, pp 1–13, 2021.

Shifat TA, Hur JW (2020) An Effective stator fault diagnosis framework of BLDC motor based on vibration and current signals. IEEE Access 8:106968–106981

Veeramuthulingam N, Ezhilarasi A, Ramaswamy M (2018) "Steady state performance enhancement strategy for brushless DC motor drive using model reference adaptive control. J Comput Theoretical Nanosci 18(3):609–619

Veeramuthulingam N, Ezhilarasi A, Ramaswamy M (2021) Torque ripple minimization effects for brushless direct current motor drive using model reference adaptive control. J Comput and Theoretical Nanosci 18(3):609–619

Zhipeng Wu, Zuo S, Huang Z, Xiaorui Hu, Chen S, Liu C, Zhuang H (2023) Effect of hall errors on electromagnetic vibration and noise of integer-slot inset permanent magnet synchronous motors. IEEE Trans on Transp Electrif 9(1):522–533